OFFICE OF NAVAL RESEARCH
CONTRACT NO. NONR 4289(01)
PROJECT NO. 384-306

TECHNICAL REPORT NO. 1

BASIC RESEARCH ON THE PROPERTIES OF MATTER USING ULTRASONIC WAVES

M. A. BREAZEALE
PRINCIPAL INVESTIGATOR

ULTRASONICS LABORATORY
DEPARTMENT OF PHYSICS

THE UNIVERSITY OF TENNESSEE
Knoxville, Tennessee

February 1966

This Technical Report consists of reprints and papers prepared in 1964 and 1965 by members of the staff and graduate students supported by the Office of Naval Research.

Staff:

M. A. Breazeale — Associate Professor of Physics

Graduate Students:

C. R. Endsley, W. R. McCluney, G. D. McNeely, A. L. Van Buren.

TABLE OF CONTENTS

I. M. A. Breazeale, "Finite Amplitude Waves in Liquids and Solids", Proceedings of the 5th ICA, Liege, Vol. Ia, D18 (1965).

II. A. L. Van Buren and M. A. Breazeale, "Distorted Wave Interaction at Boundaries", J. Acoust. Soc. Am. 38, 931 (A) (1965).

III. Charles Ross Endsley III, "A Study of Devices for the Concentration of Ultrasonic Waves", M.S. Thesis, The University of Tennessee (1965).

IV. A. L. Van Buren, "Wave Interactions at Plane Boundaries".

DISTRIBUTION LIST

5e CONGRÈS INTERNATIONAL D'ACOUSTIQUE
LIÈGE 7-14 SEPTEMBRE 1965

D18

FINITE AMPLITUDE WAVES IN LIQUIDS AND SOLIDS*

M.A. Breazeale

Department of Physics, The University of Tennessee, and
Solid State Division, Oak Ridge National Laboratory

The distortion of an initially sinusoidal ultrasonic wave recently observed in solids can be described in a way analogous to that previously used for liquids, except for certain complications associated with crystalline properties. The non-linearity parameters can be introduced in a relatively simple way if the terms in the non-linear differential equation are grouped properly. This results in a formalism which allows one to discuss non-linear effects in liquids and solids analogously and to point out parameters which differ significantly and thus characterize the two media. We have made measurements by different techniques, using results found in one medium to suggest lines of investigation in the other.

Reflection of Distorted Waves in Liquids.

It is possible to gain information about the behavior of a distorted ultrasonic wave on reflection from a boundary through the use of the diffraction of light. A 5 mc ultrasonic wave is generated in water and allowed to propagate a distance equal approximately to the discontinuity distance. At this point a reflector is placed in the water such that the distorted ultrasonic wave is reflected at an angle of approximately 15°. A beam of light from a point source passing through the water in the region of interaction of the incident and reflected waves is diffracted by both waves. The diffraction patterns resulting when one uses two extremely different reflectors are shown in Fig. 1.

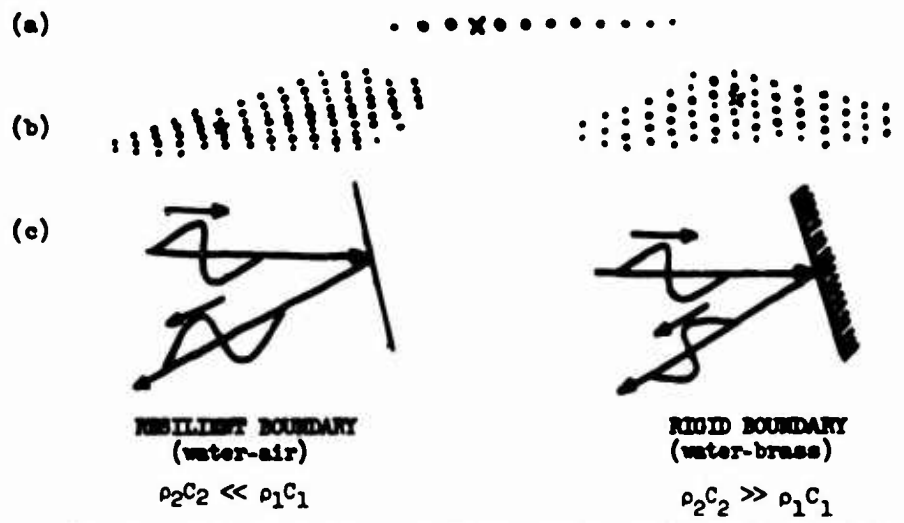

Fig. 1. Light diffraction resulting from interaction of distorted waves.

These diffraction patterns can be understood by observing the position of the zero order and realizing that the distorted ultrasonic wave behaves in much the same way as a blaze grating. The distortion in the ultrasonic waveform leads to an asymmetrical diffraction pattern. The diffraction pattern resulting from a single

*Research sponsored by the U.S. Atomic Energy Commission under contract with the Union Carbide Corporation and by the Office of Naval Research under Contract No. 4289.

distorted ultrasonic wave progressing to the right is shown in Fig. 1(a). Diffraction patterns produced in the interference region before boundaries having extreme values of acoustic impedance are shown in Fig. 1(b). These patterns can be visualized as the diffraction pattern resulting when each of the orders produced by the incident wave is diffracted by the reflected wave. The difference in the asymmetry of the pattern caused by the reflected wave produces a markedly different appearance of the overall pattern. These patterns can be explained by assuming that the distortions of the reflected waves in the two cases are as indicated in the diagram. (Fig. 1(c).) The wave reflected from a resilient boundary is distorted in a direction opposite to that reflected from a rigid boundary, and actually is now in an unstable condition because the non-linear effects now cause the higher harmonics to decrease.

These observations are consistent with what one calculates using the expression

$$\epsilon = 2 \tan^{-1} \frac{\rho_1}{\rho_2} \frac{1}{\cos \theta_1} \sqrt{\sin^2 \theta_1 - \frac{C_1^2}{C_2^2}} \qquad (1)$$

for the phase shift on reflection from an interface and assuming that the phase shift of each harmonic is the same as that of an equivalent sinusoidal wave. It should be pointed out in passing that this equation predicts the unstable waveform in the reflected wave for a rigid boundary as well as the resilient boundary when the distorted wave is at grazing incidence.

Let us consider normal incidence. If the wave is normally incident the asymmetry of the diffraction pattern indicates that standing waves are symmetrical for the rigid boundary and asymmetrical for the resilient boundary. This fact is very important in the study of solids, for the stress-free boundary condition obtaining when an ultrasonic wave impinges internally on the end of a solid is analogous to the resilient boundary discussed here. Solution of this problem of a standing finite amplitude wave in a solid could present a new means of evaluating the third order elastic constants. Such a solution is in progress. An alternative method is to consider the distortion of progressive finite amplitude waves.

Progressive Finite Amplitude Waves in Solids.

In the study of the propagation of a finite amplitude ultrasonic wave in a solid or a liquid it is usual to consider solutions to the non-linear differential equation satisfying the boundary condition that at $x = 0$, the displacement $U = A \sin \omega t$.

One can formulate the problem such that the propagation of a longitudinal ultrasonic wave in either type of medium can be described by the equation

$$\rho_0 U_{tt} = K_2(U_{xx} + 3U_x U_{xx}) + K_3 U_x U_{xx} \qquad (2)$$

where U_{tt} is the second time derivative of the displacement, and the coefficients K_2 and K_3 are introduced to make notation simple in describing a non-linear solid. For a cubic crystal the coefficients K_2 and K_3 are combinations of the ordinary elastic constants and the third order elastic constants, respectively. These combinations depend on the direction of propagation of the ultrasonic wave with respect to the crystal axes and are given for three crystal directions in Table I. For a liquid the combination $-(3K_2 + K_3)/K_2$ is replaced by $B/A + 2$, where A and B are coefficients of the Taylor expansion of the pressure in terms of the condensation. For a gas this would be $\gamma + 1$.

In deciding how much an initially sinusoidal wave will distort in propagating through a given medium, it is useful to consider the discontinuity distance L, the propagation distance required for an initially sinusoidal wave to develop a discontinuity in the particle velocity. This is given by

$$L = \frac{K_2/\rho_0}{-\left(\frac{3K_2 + K_3}{K_2}\right)(2\pi^2 f^2)\ U_0} \qquad (3)$$

where U_0 is the particle displacement amplitude at the source. As an example of

the behavior of solids compared with fluids, values of L are calculated for a 30 megacycle wave in water and for various directions in germanium. These values are given in Table II. For an assumed source amplitude $U_o = 1$ Å, a typical value of the discontinuity distance in water would be 15 cm; for germanium it would be between 120 and 500 cm depending on the direction of propagation in the crystal.

Direction	K_2	K_3
[100]	C_{11}	C_{111}
[110]	$\frac{C_{11} + C_{12} + 2C_{44}}{2}$	$\frac{C_{111} + 3C_{112} + 12C_{166}}{4}$
[111]	$\frac{C_{11} + 2C_{12} + 4C_{44}}{3}$	$\frac{C_{111} + 6C_{112} + 12C_{144} + 24C_{166} + 2C_{123} + 16C_{456}}{9}$

Table I. K_2 and K_3 for [100], [110], and [111] Directions.

Direction	K_2	K_3	L (U_o is in cm.)
[110]	1.288×10^{12} dynes/cm^2	-2.20×10^{13} dynes/cm^2	$\frac{5.04 \times 10^{-6}}{U_o}$ cm.
[110]	1.053×10^{12}	-3.93×10^{13}	$\frac{1.18 \times 10^{-6}}{U_o}$ cm.
[111]	0.9748×10^{12}	-3.36×10^{13}	$\frac{1.2 \times 10^{-6}}{U_o}$ cm.

Table II. Discontinuity Distance in Germanium.

For propagation distances small compared with the discontinuity distance, a perturbation solution of the non-linear differential equation is accurate enough to allow one to calculate the nonlinearity parameter B/A for fluids or the third order elastic constants of solids. Compared with the discontinuity distances calculated above it is clear that the ultrasonic path in solid samples of ordinary sizes would be quite small so that a perturbation solution of Eq. 1 should be quite accurate. Therefore, when the distortion of the finite amplitude wave is large enough to measure, this should be an accurate means of determining the third order elastic constants of solids provided the attenuation can be controlled sufficiently.

A perturbation solution of Eq. 2 in terms of the discontinuity distance L is

$$U = U_o \sin(kx - \omega t) + \frac{U_o x}{2U_o L} \cos 2(kx - \omega t) + \ldots \qquad (4)$$

This solution predicts that the second harmonic in a distorted ultrasonic wave is proportional to the distance from a sinusoidal driver and proportional to the square of the fundamental amplitude. These functional relationships serve as a check on experiment and as a means of determining whether absorption is negligible as has been assumed.

Measurements have been made on [111] samples of copper single crystals using a pulse technique. Results of measurements of the first transmitted pulse in an

annealed 9.1 cm sample of copper are given in Fig. 2, which is a log-log plot of the amplitudes of the second harmonic and the fundamental, relative to an arbitrarily established reference, as a function of source amplitude. It is seen that there is a considerable range of source amplitudes for which the second harmonic curve has a slope of 2 which is expected if there is a square relationship between them.

In Fig. 3 is given the distance dependence of the second harmonic using samples of various lengths. Note that the above results on liquids show that one cannot simply use successive reflections in the same sample to study path length dependence, since on each return trip the second harmonic is generated with phase opposite to that produced by reflection, with the result that the wave "undistorts". The behavior before and after a neutron bombardment of 3.6×10^{15} neutrons/cm^2 is shown. One sees that the amplitude of the second harmonic increases with distance as it should. Further, the expected linear increase with distance is improved after bombardment. As the distance increases the second harmonic evidently is approaching a maximum value; however it appears that at shorter distances the curve is reasonable linear, in agreement with theoretical predictions. The rapid initial increase in the pre-bombardment second harmonic can be attributed to the non-linear interaction of dislocations,[3] which evidently reduces the effective discontinuity distance. Neutron bombardment appears to reduce this dislocation interaction in copper to the point that the effects of the non-linearity of the crystal lattice become dominant.

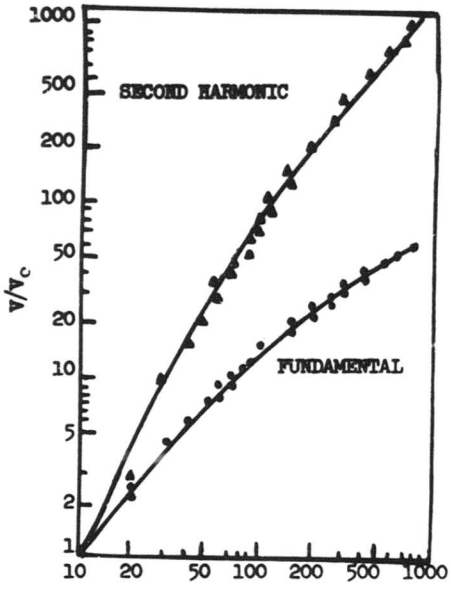

Fig. 2. Behavior of Fundamental and second harmonic in annealed [111] copper sample as function of source amplitude.

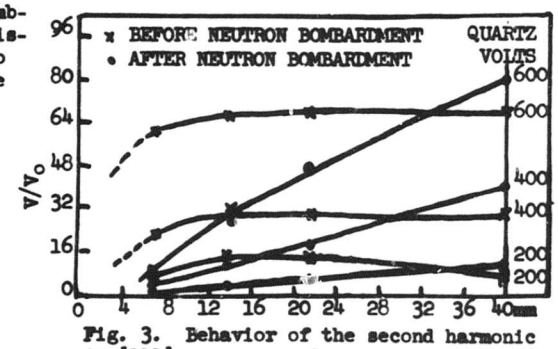

Fig. 3. Behavior of the second harmonic in [111] copper samples as function of distance, showing the effect of neutron bombardment.

REFERENCES

1. A.A. Gedroits and V.A. Krasil'nikov, J. Exptl. Theoret. Phys.(USSR), 43, 1592 (1962).
2. M.A. Breazeale and D.O. Thompson, Appl. Phys. Lett., 3, 77 (1963).
3. A. Hikata, B. Chick and C. Elbaum, Appl. Phys. Lett., 3, 195 (1963).

Distorted Wave Interaction at Boundaries*

A. L. Van Buren
and
M. A. Breazeale
Department of Physics, The University of Tennessee
Knoxville, Tennessee

When a distorted ultrasonic wave is reflected from a boundary, interesting phenomena can arise. For example, if the harmonics are shifted in phase relative to each other by the right amount, then the reflected wave can actually be distorted backward. On further propagation the same phenomenon which caused the wave to become distorted in the first place now "undistorts" the wave and the waveform again approaches a sinusoid. In a nondispersive medium these modified phase relations between the harmonics will be maintained until this undistortion is completed. The change of phase of each of the harmonics upon reflection from the surface is the cause of this phenomenon. In the case of a sinusoidal wave, when the angle of incidence is greater than a critical angle, a phase shift occurs that is dependent on the character of the boundary and on the angle of incidence. One can now study the non-sinusoidal case and make some assumptions about the relation

---

*Presented at the 70th meeting of the Acoustical Society of of America. (J. Acoust. Soc. Am. 38, 931 (A) (1965.)

between the sinusoidal and nonsinusoidal cases.

Since the non-sinusoidal case is a non-linear phenomenon, strictly speaking, superposition is not completely valid, so that the results of such a study will be a test of both the linear theory and the approximations to the non-linear theory.

In our theoretical consideration we assumed that the Fourier components of the distorted wave were reflected in the same way as a sinusoidal wave of the same frequency. We can test this assumption by comparison of phase shifts measured in distorted waves with those calculated from theory.

If a reflected ultrasonic pulse is monitored by a transducer tuned to the second harmonic, and if the amplitude is not too great, then the received signal can be analyzed in terms of only a fundamental and a second harmonic term. In this case the phase angle between the two harmonics as seen by the second harmonic is equal to the phase shift upon reflection plus a constant phase difference for all angles of incidence.

Expressions for the complex ratio of the amplitude of the reflected wave to that of the incident wave have been developed from linear theory consideration. Lord Rayleigh considered the linear wave interaction at a liquid-liquid interface and obtained an expression for the phase shift of the reflected wave relative to the incident wave. Here

only longitudinal waves need be considered. Therefore, the expression is relatively simple.

In the case of the liquid-solid interface, however, shear waves in the solid must be considered, and the resulting expressions become more complicated. This problem was considered by Knott. Use of his equations lead to the reflectance as given by Ergin in 1952. One can rewrite this expression for two major regions, one region between the critical angle for the longitudinal wave and the critical angle for the shear wave; the other region from the shear critical angle to grazing incidence. This results in a complex ratio with the phase shift given in the usual manner. For the theoretical curves then, we have considered only linear theory while the distortion itself is a nonlinear phenomenon.

The experimental apparatus involved a pulsed two transducer system, each transducer being mounted on an arm free to rotate about a central axis. A reflector was immersed in the liquid. Its face was placed along the axis of the system so that once alignment was obtained for one angle, the arms could be rotated to another angle, and alignment would be maintained. The angle was measurable to within one tenth of a degree by use of a calibrated scale mounted on the central rod. Alignment was achieved for normal incidence by use of the same transducer as a transmitter and a receiver. The received waveform was

monitored by a transducer tuned to the second harmonic. This accentuated the second harmonic and thus allowed the use of more moderate amplitudes. At each angle of incidence the amplitude was decreased until the monitored waveform was sinusoidal. Then the arm containing the receiver was rotated until the maximum signal was received. Now the received waveform represented the reflected wave for the measured angle of incidence. At larger amplitudes then the received waveform for various angles of incidence was monitored and photographed.

The waveforms were then synthesized by using two audio signal generators. The phase difference was then obtained from the resulting Lissajous pattern when the synthesized waveform was identical to the reflected waveform. The correction to the phase shift was obtained from the case where no phase shift occurs upon reflection. Amplitudes were also obtained but involved the frequency response of the receiving transducer.

Of the parameters involved in the theoretical expressions, the only one involving difficulty in measuring is the velocity of the shear wave in the solid. This was obtained with the same apparatus by measuring the received amplitude when the output voltage was very low so that the received waveform was distorted. As the critical angle was approached the reflectance increased sharply reaching unity exactly at the critical angle. This method leads to measurements of the critical

angle to within three tenths of a degree.

Figure 1 gives the phase shift for a water-brass interface. The solid curve is the theoretical curve while the triangles represent the experimental points. Note the two critical angles. After the first critical angle we begin to obtain non-zero phase shifts. The location of what we call the transition region here is largely determined by the location of the shear critical angle. It is interesting that almost all of the experimental points lie outside the theoretical curve.

Figure 2 gives the results for a water-aluminum interface. The important feature is that the qualitative relation of the experimental points to the theoretical curve is the same as for the water-brass interface. Again the transition region occurs earlier for the experimental data.

However, this discrepancy is real and probably not the result of the experimental method. As an example of this, consider the transition region. To bring the transition region of the theoretical curve into conjunction with that of the experimental points would require over a 10% change in the shear velocity. Thus the discrepancy probably lies in the expressions for the phase shifts. Of course, the discrepancy between theory and experiment is not so great if we consider the assumptions that were made, particularly those of linearity and independent reflection of each harmonic.

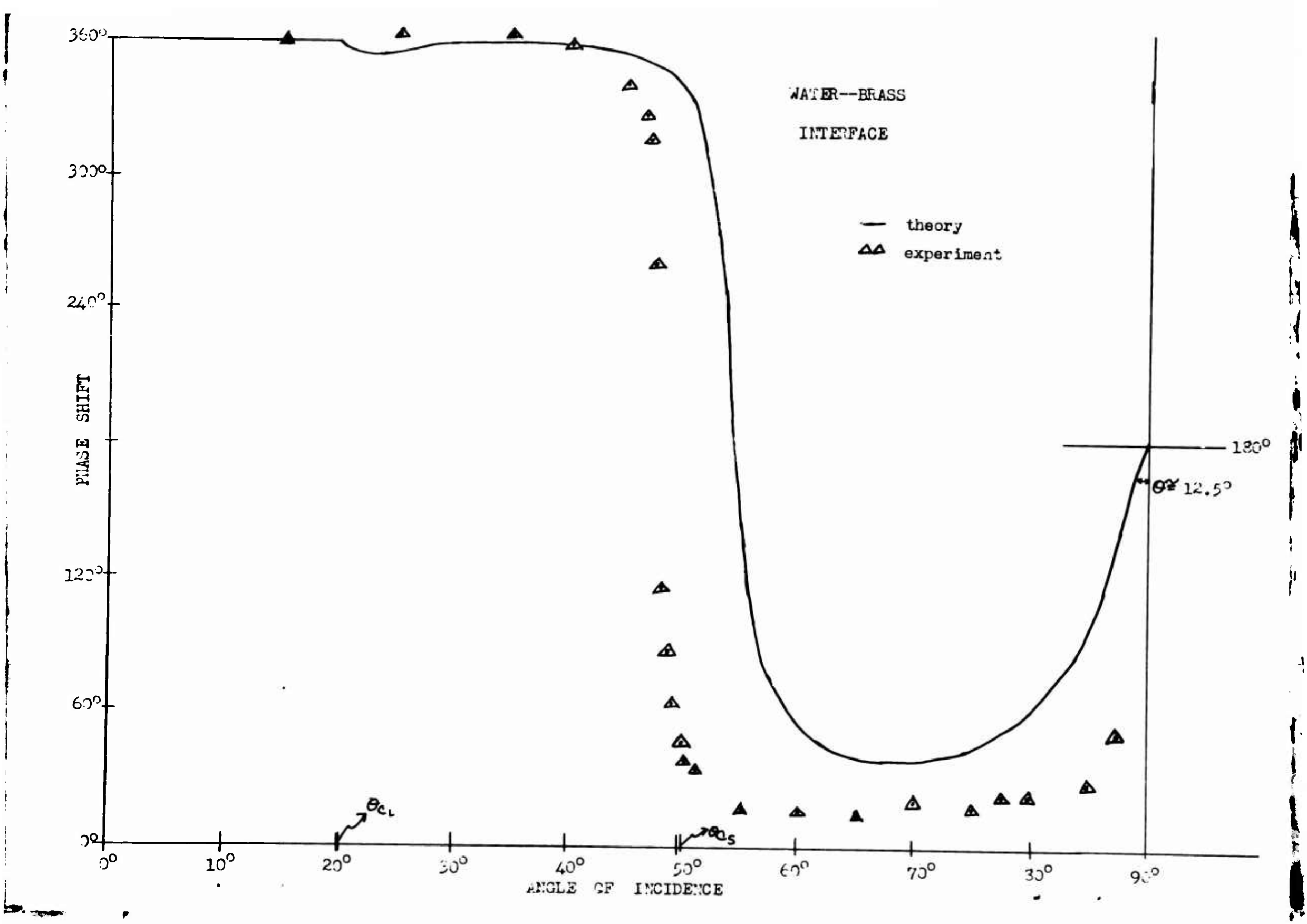
WATER--BRASS
INTERFACE
theory
experiment
PHASE SHIFT
360°
300°
240°
120°
60°
0°
180°
12.5°
0°
10°
20°
30°
40°
50°
60°
70°
80°
90°
ANGLE OF INCIDENCE

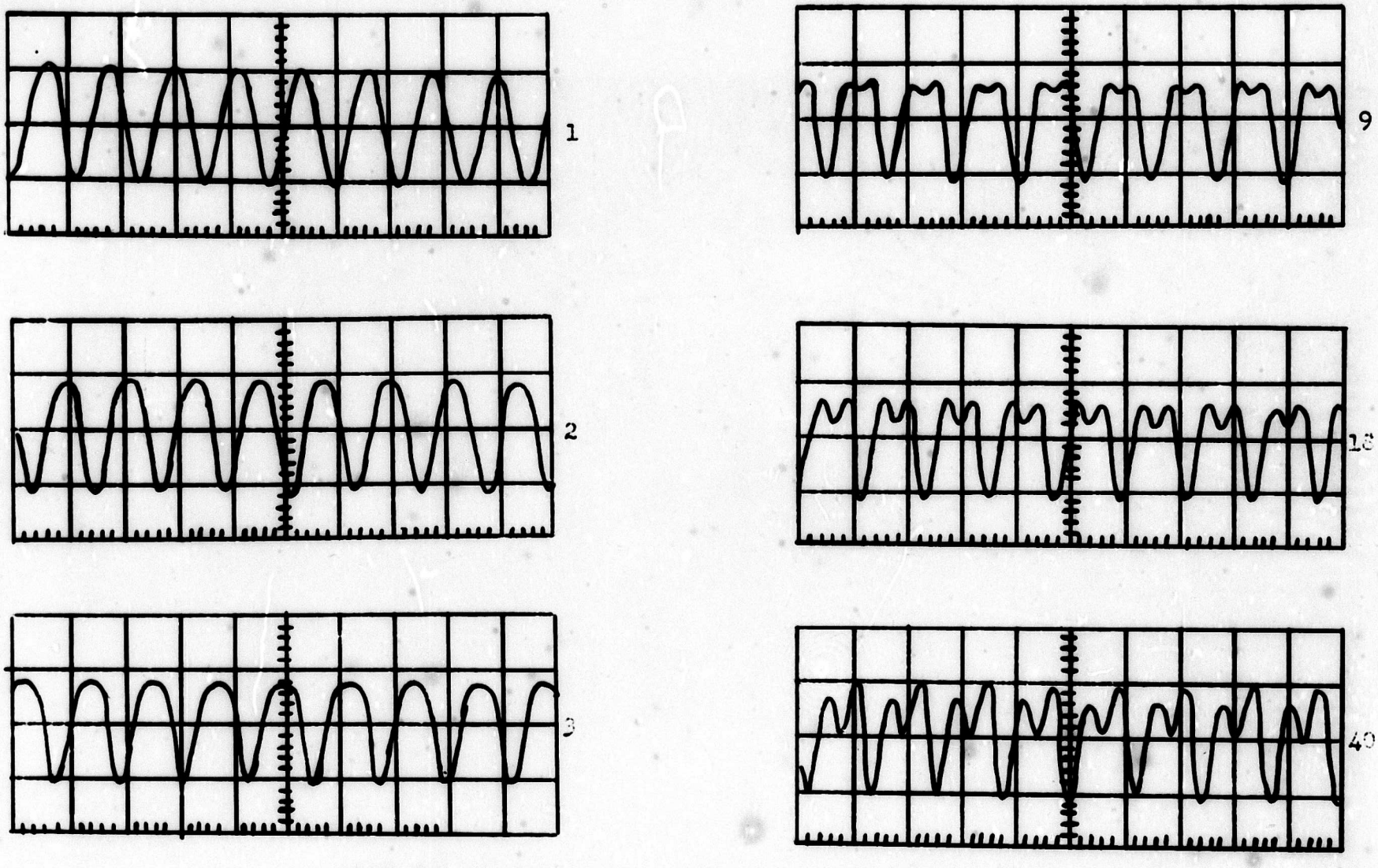

REFLECTED WAVEFORMS FOR VARIOUS REL. SOUND PRESSURES

(water-aluminum interface with $\alpha = 30.3°$)

Figure 2

Let us now look at the effect of amplitude on the phase shifts. Figure 3 shows the reflected waveform for various relative pressures for an angle of incidence of 30.3° in the case of water-aluminum. This angle corresponds to the transition region as measured experimentally. This waveform was chosen because of its symmetry. If the phase relation between the fundamental and the second harmonic remains constant as the pressure is increased then the symmetry should be maintained. Note that except for the last case where a very large acoustic pressure was present the waveforms are all symmetrical indicating no relative phase shift of the harmonics with amplitude. The pressures used in the experiments were far below that represented by the last waveform which corresponds to a pressure of > 7 atmospheres. If one neglects losses, this pressure is calculated at 24 atmospheres. Thus it appears that the effects are not a function of amplitude.

Figure 4 shows the results for a water-glycerin interface. Experimentally this was effected by use of a thin sheet of a polymer between the water and the glycerin. The unit containing the glycerin was also placed at the central axis. The discrepancy between theory and experiment is very marked. However, problems exist in alignment, particularly due to the fact that the polymer was never truly planar because of the effects of glycerin on it as well as its tendency to stretch. Use of mica or another fairly rigid material as a separator will solve

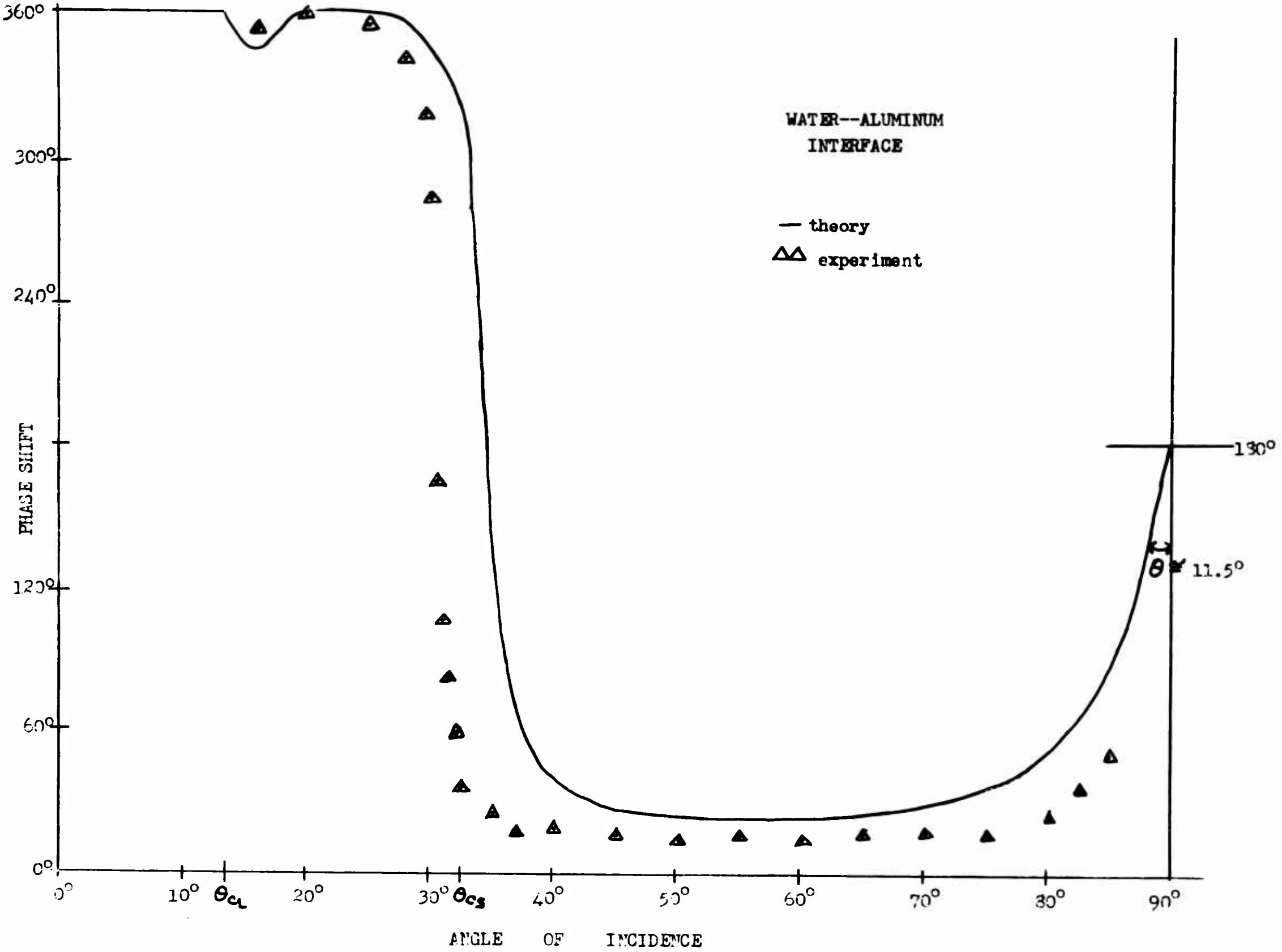
WATER--ALUMINUM
INTERFACE
— theory
ΔΔ experiment
360°
300°
240°
120°
60°
0°
PHASE SHIFT
130°
θ
11.5°
0°
10°
θcl
20°
30°
θcs
40°
50°
60°
70°
80°
90°
ANGLE OF INCIDENCE

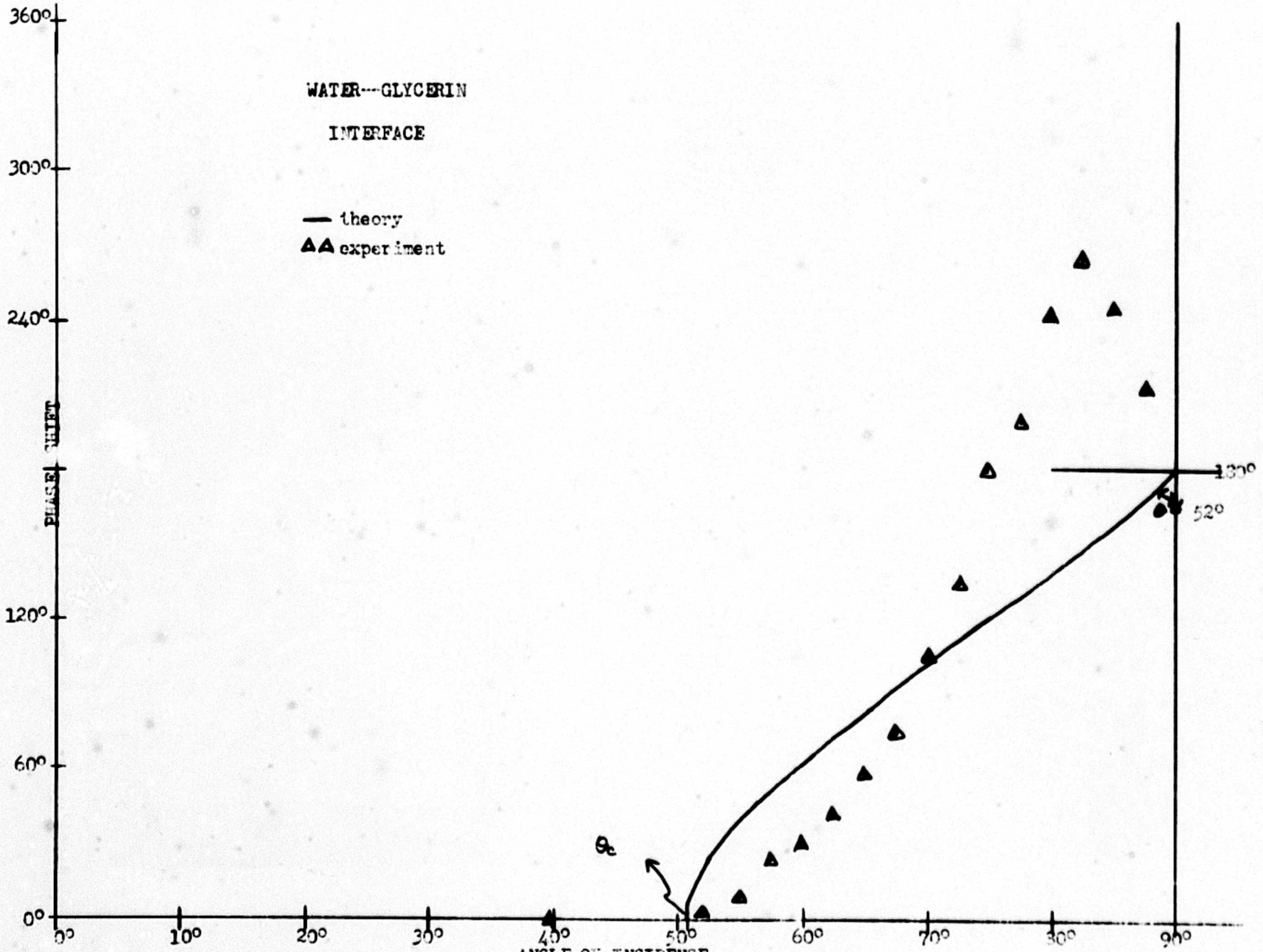
WATER---GLYCERIN
INTERFACE
theory
experiment
360°
300°
240°
120°
60°
0°
PHASE SHIFT
0°
10°
20°
30°
40°
50°
60°
70°
80°
90°
ANGLE OF INCIDENCE
θc
130°
52°
Figure 4

this problem in the future.

Yet the scatter of the experimental points is rather small and indicates that the linear theoretical expression is inadequate. There is an entirely different curvature for the first half of the curve. This agrees qualitatively with the curvature of the phase shift measurements made by Gessert and Hiedemann for glycerin to carbon-tetrachloride by stroboscopic techniques.

The rest of the curve is drastically different however, since the phase shift rises above 130° and then approaches 130° as the angle of incidence approaches 90° whereas the theoretical phase shift is never greater than 130° and is monotonically increasing with angle of incidence. We know that Rayleigh waves and other surface waves may occur in the polymer for specific angles of incidence. The region in the vicinity of these two points may correspond to the region where these waves are produced.

In conclusion then, it appears that this method of measuring phase shifts gives precise results, but that a gap exists between the experimental results and theoretical expressions based on the obvious extensions of linear theory.

A STUDY OF DEVICES FOR THE CONCENTRATION OF ULTRASONIC WAVES

Charles Ross Endsley III, M. S.

Department of Physics
Ultrasonics Laboratory
The University of Tennessee
Knoxville, Tennessee

August, 1965

TABLE OF CONTENTS

CHAPTER		PAGE
I.	INTRODUCTION.	1
II.	AN ULTRASONIC EXPONENTIAL HORN.	3
	Design.	3
	Simplified Horn Theory.	5
	The Radiation Past the Throat	8
	Experimental Procedure.	11
	Discussion of Results	11
III.	AN ULTRASONIC ZONE PLATE.	18
	Design.	18
	The Fresnel Field	18
	Experimental Procedure.	20
	Discussion of Results.	20
IV.	SUMMARY AND CONCLUSIONS.	23
BIBLIOGRAPHY.		24

LIST OF FIGURES

FIGURE		PAGE
1.	Design of the Exponential Horn	4
2.	Slit for Calculating the Radiation Pattern from the Throat.	9
3.	Predicted Radiation Pattern for Medium Horn.	10
4.	Acoustical Apparatus for Testing the Exponential Horn	12
5.	Schlieren Photograph of the Sound Field in the Small Horn.	13
6.	Schlieren Photograph of the Sound Field in the Medium Horn	15
7.	Schlieren Photograph of the Sound Field in the Large Horn.	17
8.	Design of the Ultrasonic Zone Plate.	19
9.	Schlieren Photograph of the Focus of the Ultrasonic Zone Plate	22

A STUDY OF DEVICES FOR THE CONCENTRATION OF ULTRASONIC WAVES*

Charles Ross Endsley III
Department of Physics
The University of Tennessee
Knoxville, Tennessee

I. INTRODUCTION

One of the aims of the Ultrasonics Group is the study of the physical effects of finite amplitude ultrasonic waves. It is known that the nonlinear term in the differential equation describing the density of the medium is large enough to produce certain types of distortion of the waveform when the amplitude is very large; however, it has been pointed out by Naugolnykh (1964) that even for very small amplitudes, if the wave front is spherical, the nonlinearity of the medium will become very important at the center of curvature where the waves come to a focus. It was therefore decided to study the focussing properties of certain well-known devices with the idea that later detailed investigations of the nonlinear behavior at the focus could be made. Two devices were studied: an exponential horn and a zone plate. It turned out that special adaptations of both of these devices had to be made in order to use the schlieren optical technique to

---

*This report is an excerpt from a thesis presented to the Graduate Council of The University of Tennessee in partial fulfillment of the requirements for the Degree of Master of Science. The work described was done under contract 4289 (01) with the Office of Naval Research.

study their focussing properties. This report is a description of experiments made in the study.

The exponential horn is probably used most often as a device to match the impedance of a driver in a loudspeaker system to the impedance of the surrounding air. This type of horn can be turned around, however, and used to concentrate sound energy. Mason and Wick (1951) used a solid exponential horn to increase the amplitude of vibration by a factor of ten. Krassilnikov (1963) describes this same idea in less detail, and Makarov (1964) discusses the finer details of the design of such a horn. These horns were designed for low frequencies and were only a few half-wavelengths long. For example, Mason's horn was half a wavelength (at 18 k.c.) long and the medium transmitting the energy in the horn was brass. The horn to be discussed here, however, is 134 wavelengths (at 2 mc.) long and uses water as the transmitting medium. This results in a presentation somewhat different from that for the solid horn.

The pattern of sound waves emerging from the small end of the horn was found to be similar to the pattern for plane waves going through a single slit. Photographs of single slit diffraction can be found in Bergmann (1954) and Hiedemann (1939). These same references contain photographs of Fresnel zones of single slits which may be compared with the Fresnel zone of the central slit of the zone plate; however, a photograph of ultrasonic waves focussed by a zone plate was not published.

An ultrasonic zone plate behaves in the same way as an optical one. The principles of operation of an optical zone plate can be found in almost any general optics text such as Jenkins and White (1957). The focus of the zone plate can be compared with the focus of a lens; however, it is impossible to photograph the optical wave field near the focus. On the other hand, photographs of the wave field near the focus of an ultrasonic zone plate can be readily made using the schlieren technique.

II. AN ULTRASONIC EXPONENTIAL HORN

Design

The first horn was built of brass and was of circular cross-section. The patterns coming from the throat were observed by the schlieren technique. However, the gain in intensity predicted by the simplified horn theory was not observed. Therefore, the horn was redesigned so that the sound field inside the horn could be investigated. It was redesigned as in Fig. 1 with a rectangular cross-section leaving both sides open so that the sound field could be observed by the schlieren technique. It was also designed so that the separation of the top and the bottom halves could be varied. These adjustments made possible a departure from a true exponential horn but did not affect the focussing properties markedly, although they did affect the way the ultrasonic waves emerged from the horn, as will be shown.

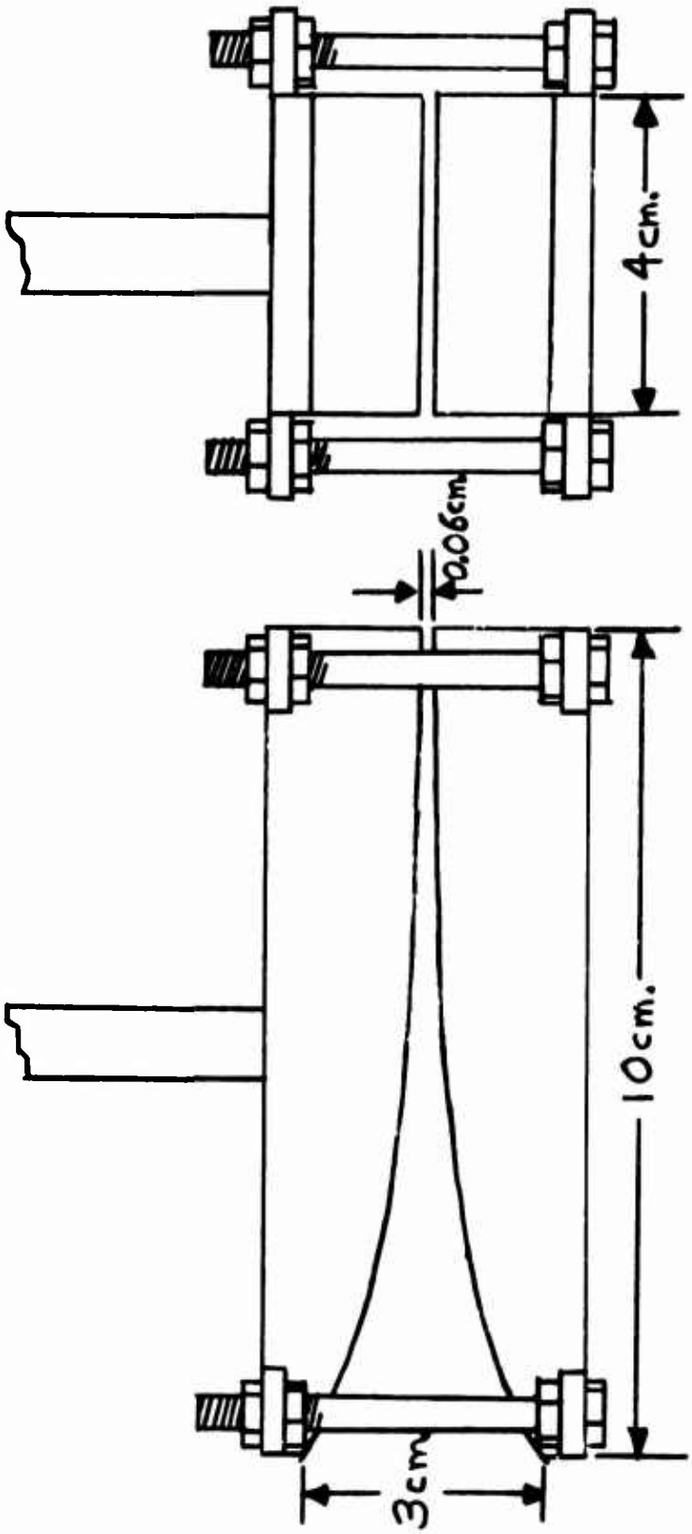

Figure 1. Design of the Exponential Horn.

The cross-sectional area of the horn was of the form

$$S = S_o e^{-mx} , \tag{1}$$

where S is the cross-sectional area at a distance x from the mouth, and S_o is the cross-sectional area of the mouth. For the case when the width is constant, equation (1) can be written as

$$y = y_o e^{-mx} , \tag{2}$$

where y is the half-separation. The horn was designed with a flare constant m = .391 and with a half width at the throat y_o = 1.5 cm.

Simplified Horn Theory

Horns for audible sound waves in air are normally used to increase the effective radiating area of a small piston. Here the piston, producing approximate plane waves, is placed at the throat. The waves then emerge at a lower intensity at the mouth of the horn. However, the waves are no longer plane waves but have wave fronts whose shape depend on the configuration of the horn.

Since the horn under consideration was made to accept plane waves at its mouth rather than its throat, the situation was quite different from the audible case discussed above. The most obvious difference is that the surfaces of equal phase at the mouth are now planar. Kinsler and Frey (1950) give a simplified horn theory which can be adapted to this new situation. This theory is dependent on the following assumptions: (1) the medium is completely linear for the amplitude of vibrations under consideration; (2) the sound waves begin as plane waves and remain plane throughout the horn; and (3) the horn

walls are perfectly rigid. These considerations lead to the wave equation for horns:

$$\frac{\partial^2 u}{\partial t^2} = c^2 \frac{\partial}{\partial x}\left[\frac{1}{S_x}\frac{\partial}{\partial x}(S_x u)\right], \tag{3}$$

where u is the particle displacement, and S_x is the cross-section at x.

In order to make equation (3) applicable to an exponential horn, equation (1) is substituted for S_x giving:

$$\frac{\partial^2 u}{\partial t^2} = c^2\left[\frac{\partial^2 u}{\partial x^2} - m\frac{\partial u}{\partial x}\right]. \tag{4}$$

Assuming a solution of the form:

$$u = A e^{j(\omega t + \gamma x)}, \tag{5}$$

it is found upon substitution that the allowed values of γ are:

$$\gamma = j\frac{m}{2} \pm \sqrt{k^2 - m^2/4}. \tag{6}$$

Letting $\alpha = \frac{m}{2}$ and $\beta = \sqrt{k^2 - \frac{m^2}{4}}$, the general solution of equation (4) can be written as:

$$u = e^{\alpha x}\left[A e^{j(\omega t - \beta x)} + B e^{j(\omega t + \beta x)}\right]. \tag{7}$$

The schlieren technique used to view these waves responds to change in density relative to the density of the undisturbed medium. This means the effect depends on the condensation or, in like manner, on the acoustic pressure which is:

$$p = -\rho_0 c^2 \frac{\partial u}{\partial x} = j\rho_0 c^2 \alpha\beta e^{\alpha x}\left[A e^{j(\omega t - \beta x)} - B e^{j(\omega t + \beta x)}\right] \quad . \quad (8)$$

The factor $e^{\alpha x}$ in this expression represents the increase in pressure produced by the corresponding decrease in cross-sectional area. The expression in brackets represents a standing wave produced by the interference of the two oppositely travelling waves. The schlieren pattern for the standing wave should consist of lines perpendicular to the direction of propagation and spaced a half wavelength apart. Thus, the simplified horn theory predicts a standing wave pattern superimposed on a field of exponentially increasing intensity as the distance from the mouth increases.

According to Morse (1948) good transmission depends on minimum reflection from the walls of the horn. Reflections tend to cause energy to be trapped and dissipated in the horn. Thus, the particle velocities near the walls should always be parallel to the walls. A horn with plane waves incident at the mouth will cause reflections. At the very mouth of the horn the angle of incidence on the walls of the horn is 59.6°; whereas for good transmission through the horn, it should be nearer 90°. It should, therefore, be expected that energy will be trapped in the horn under consideration. The schlieren

photographs verify this and show the positions at which this occurs.

The Radiation Past the Throat

The radiation pattern past the throat is very similar to the radiation pattern which would be obtained by passing plane waves through a slit even though the waves emerging from the throat are not plane. The single slit case will be treated here, and then differences between the two situations will be discussed.

Assume plane waves passing through a slit of length ℓ and width a as shown in Fig. 2. The element of pressure contributed by the strip of width dz and length ℓ along the y axis can be found by integrating the contributions to the pressure from each area element dydz. (For the case $y^2 << r^2$) this results in the following equation:

$$dp = \frac{j\rho_0 c k U_0}{2\pi r} e^{j(\omega t - kr)} \frac{a \sin\beta}{\beta} dz \quad , \qquad (9)$$

where k is the wave constant, U_0 is the velocity amplitude of the surface element, and $\beta = \frac{ka}{2 \sin\theta}$. The term $\frac{a \sin\beta}{\beta}$ is the familiar expression for the variation of light amplitude with angle for a single slit diffraction pattern (Jenkins and White, 1957). Since in the linear approximation the relation between pressure and condensation is $P = \rho_0 c^2 S$, the condensation amplitude at P varies with angle just as the pressure does.

Equation (9) gives only the contribution of the strip element lying along the y-axis; however, it should be adequate to explain the patterns obtained. Justification of this assumption is found in the qualitative agreement between the theory and the experimentally

photographs verify this and show the positions at which this occurs.

The Radiation Past the Throat

The radiation pattern past the throat is very similar to the radiation pattern which would be obtained by passing plane waves through a slit even though the waves emerging from the throat are not plane. The single slit case will be treated here, and then differences between the two situations will be discussed.

Assume plane waves passing through a slit of length ℓ and width a as shown in Fig. 2. The element of pressure contributed by the strip of width dz and length ℓ along the y axis can be found by integrating the contributions to the pressure from each area element dydz. (For the case $y^2 << r^2$) this results in the following equation:

$$dp = \frac{j\rho_0 c k U_0}{2\pi r} e^{j(\omega t - kr)} \frac{a \sin\beta}{\beta} dz \quad , \qquad (9)$$

where k is the wave constant, U_0 is the velocity amplitude of the surface element, and $\beta = \frac{ka}{2 \sin\theta}$. The term $\frac{a \sin\beta}{\beta}$ is the familiar expression for the variation of light amplitude with angle for a single slit diffraction pattern (Jenkins and White, 1957). Since in the linear approximation the relation between pressure and condensation is $P = \rho_0 c^2 S$, the condensation amplitude at P varies with angle just as the pressure does.

Equation (9) gives only the contribution of the strip element lying along the y-axis; however, it should be adequate to explain the patterns obtained. Justification of this assumption is found in the qualitative agreement between the theory and the experimentally

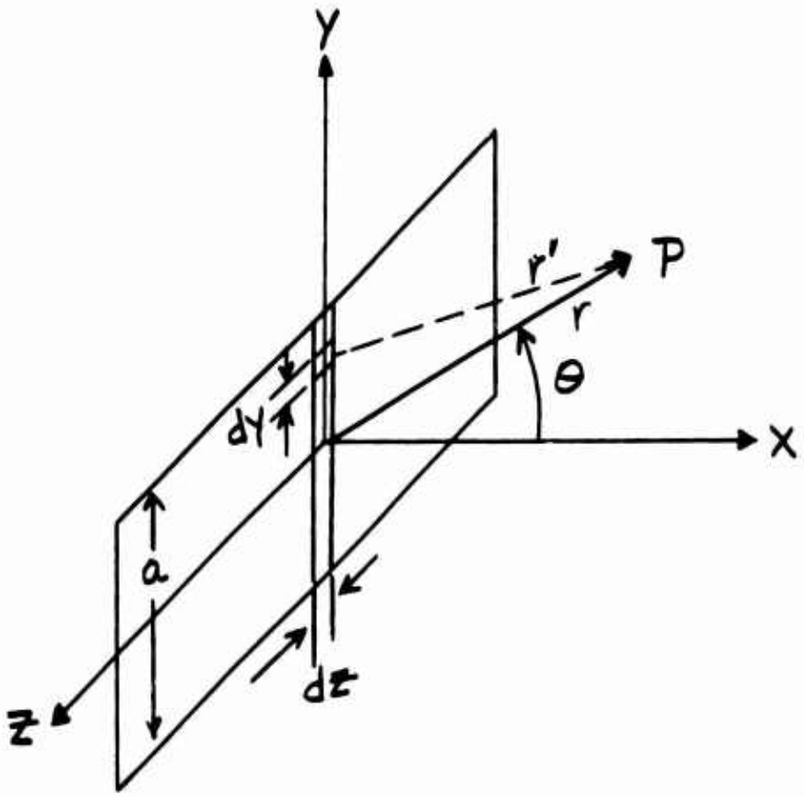

Figure 2. Slit for Calculating the Radiation Pattern from the Throat.

observed radiation patterns described later in the paper. Consider the dependence on θ as given by the term $\frac{\sin\beta}{\beta}$. In order to more conveniently represent this graphically, the expression $\log_{10}\frac{\sin\beta}{\beta}$ is plotted versus θ in Fig. 3 for the case $\frac{\lambda}{a} = .329$.

For these conditions of $\frac{\lambda}{a}$, we refer to the horn as a medium horn. Values of $\frac{\lambda}{a} = 1.16$ and 0.230 refer to the small horn and large horn respectively. Plots of $\log_{10}\frac{\sin\beta}{\beta}$ for the other horns are similar to Fig. 3 although there is only one lobe in the case of the small horn.

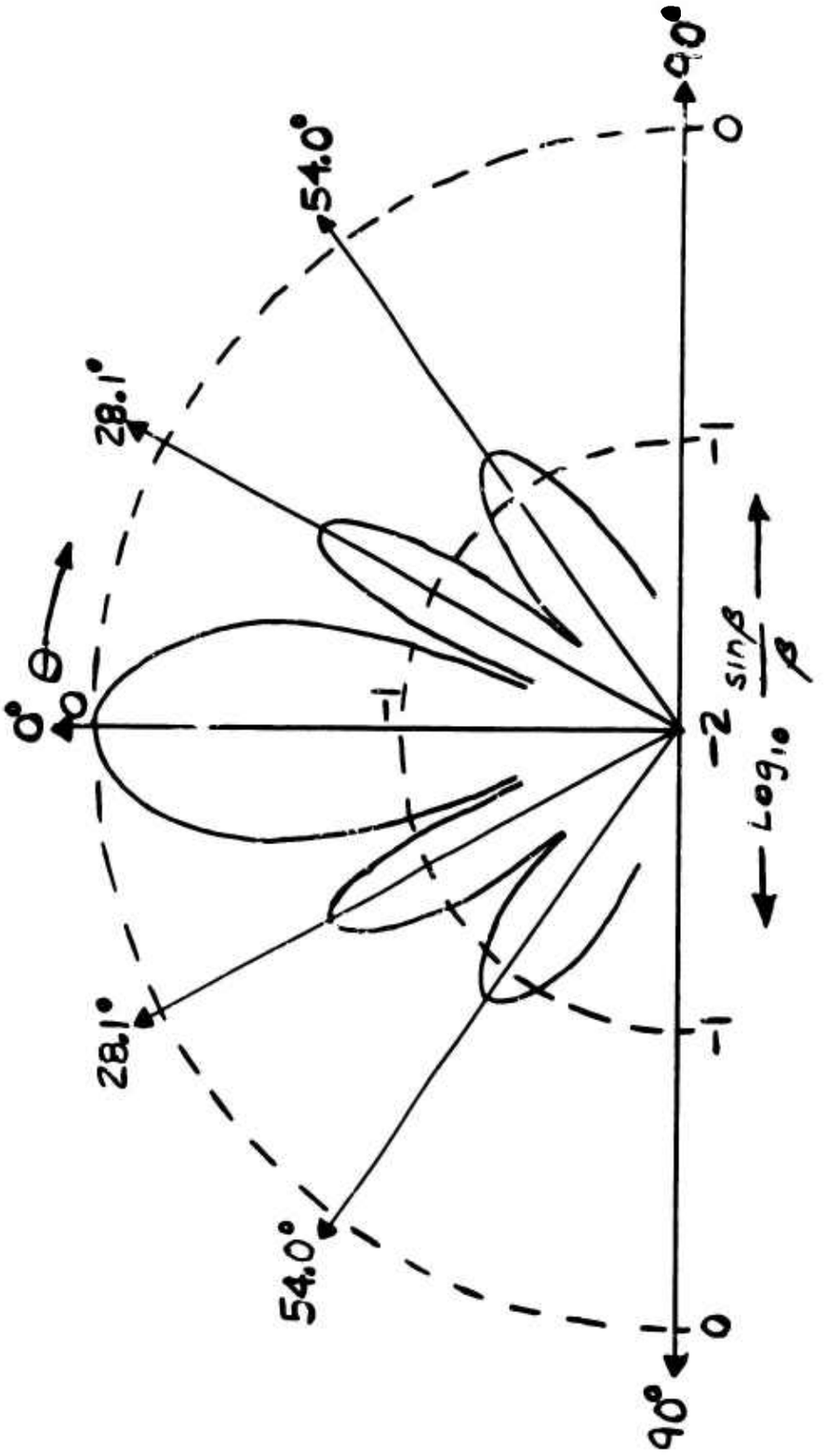

Figure 3. Predicted Radiation Pattern for Medium Horn.

Experimental Procedure

The horn and crystal transducer were centered in the test area of a schlieren system and aligned so that the sound beam passed through the light beam at normal incidence. This arrangement is shown in Fig. 4. The sound beam was adjusted parallel to the axis of the horn, by obtaining a symmetrical pattern inside the horn.

The intensity of the source was adjusted so that the pattern inside the horn could be seen with maximum contrast and detail. Starting just outside the mouth of the horn, frames were taken of sections of the horn such that each frame would overlap the preceeding frame. Upon reaching the throat, a frame was taken of the pattern radiated from the throat.

The first run was made with the horn adjusted for 0.162 cm. separation. The horn with this adjustment is referred to as the "medium horn". Succeeding runs were made with separations of 0.064 cm. (small horn) and 0.324 cm. (large horn).

Discussion of Results

Figure 5 is the small horn with $\frac{\lambda}{a} = 1.162$. First, it is obvious that reflections are present and there is an interference pattern inside the horn. The threads on the post at the mouth of the horn were always toward the upper wall of the horn. The small hemispheres along the top are bubbles caused by cavitation at a higher intensity than that used for this photograph. This cavitation was recognized as one of the problems in achieving good transmission with the first horn

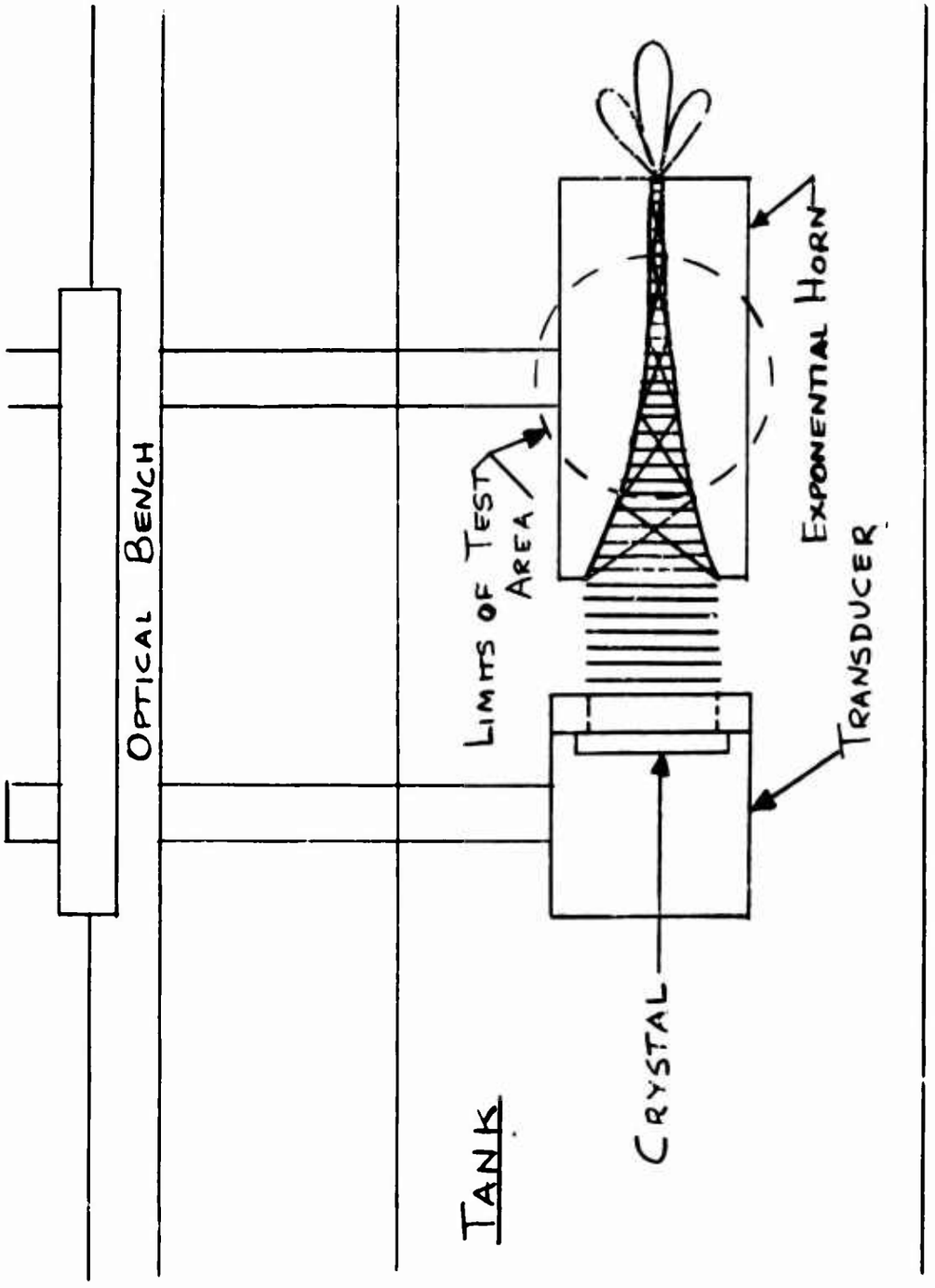

Figure 4. Acoustical Apparatus for Testing the Exponential Horn.

Figure 5. Schlieren Photograph of the Sound Field in the Small Horn.

of circular cross-section. Cavitation was evidently produced at the regions of high intensity, and the bubbles caused reflections within the horn. The interference pattern in the horn does not start along the axis of the horn until some place behind the front post. This is as it should be because the waves first reflected at the very front of the horn are reflected at an angle of 30.4° from the surface of the walls, which are inclined at an angle of 30.4° from the horizontal at this point. By geometry it is found that a reflection from this point will reach the axis of the horn at 0.84 cm. from the mouth, just behind the post in all photographs of the horn. The interference pattern itself is quite symmetrical in all the pictures. It can also be seen that there are many positions within the horn at which energy is concentrated and dissipated. The pattern at the end of the horn in Fig. 5 has only one lobe as predicted by theory.

Figure 6 is a photograph of the medium horn. It was taken using a higher sound intensity than in any of the other photographs. The interference pattern within the horn shows even more clearly in the medium horn than in the small horn. The spots of high intensity in the pattern near the mouth are arranged in smooth curves from top to bottom. These curves are similar to the surfaces of equal phase in the coordinate system given by Morse (1948). The surfaces of equal phase in that coordinate system can only be produced when no reflections occur and no interference pattern is present. However, the interference pattern can give insight into the relative phases at different points. Hiedemann and Breazeale (1959) give a schlieren photograph of

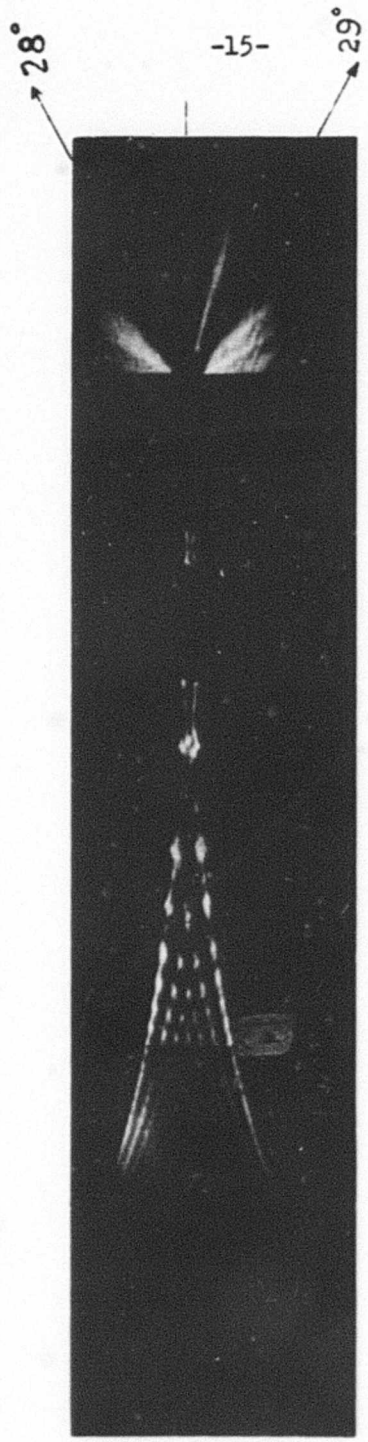

Figure 6. Schlieren Photograph of the Sound Field in the Medium Horn.

a similar interference pattern. They show a stroboscopic photograph of the same field, which shows that the surfaces of equal phase are alternately corrugated and discontinuous in such a field.

Figure 3 is the predicted pattern at the throat of the medium horn. This shows that the side lobe on either side should be expected at an angle of 28.1° from the central lobe and another at 54°. The average of the angles of the side lobes in Fig. 6 is 29.5°. The second set of lobes at 54° in Fig. 3 is very faint in the photograph.

Figure 7 is a photograph of the large horn. This photograph shows minute detail of the pattern within the horn and the pattern outside the throat. The irregularity of the pattern near the throat is caused by heat schlieren.

The pattern past the throat shows lobes at approximately 19.5° (an average of the two angles). The theory predicts that the first side lobes will be at 19.30°, which indicates close agreement with experimental results. The other two pairs of side lobes predicted by theory were too weak to be detected with this setting of the schlieren slit. The agreement between calculated and measured lobe angles points out that the shape of the wave front emerging from the throat actually has little effect on this characteristic of the single slit diffraction pattern.

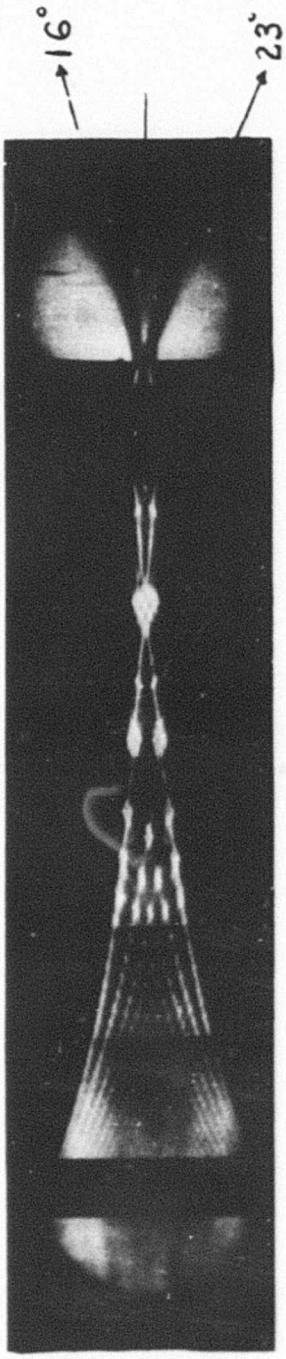

Figure 7. Schlieren Photograph of the Sound Field in the Large Horn.

II. AN ULTRASONIC ZONE PLATE

Design

An ultrasonic zone plate was designed so as to focus ultrasound in the same way that an optical zone plate focusses light. This zone plate is shown in Fig. 8. As can be seen, it was designed such that the focus would be along a line parallel to the slits in the plate rather than at a point. The actual slit widths and separations were determined from the following considerations of the Fresnel pattern behind the zone plate.

The Fresnel Field

Consider the zone plate shown in Fig. 8 with the distance from the center given by x. Let plane waves be incident from the left. If a focus is desired at a point on the axis a distance "a" from the zone plate, the contributions from all the slits in the zone plate must be in phase at that point. Thus, the path lengths to the slits must differ by an integral number of wavelengths. The width of the slits is determined by requiring that the distances to the focus from the opposite sides of the slit differ by a half wavelength. Thus, the distance of all the edges can be combined into the expression $a + \frac{n\lambda}{2}$ (n is an integer). If $a \gg n\lambda$, the expression can be solved to give

$$x = \sqrt{an\lambda} \tag{11}$$

This is the equation governing the widths and locations of the slits in the plate.

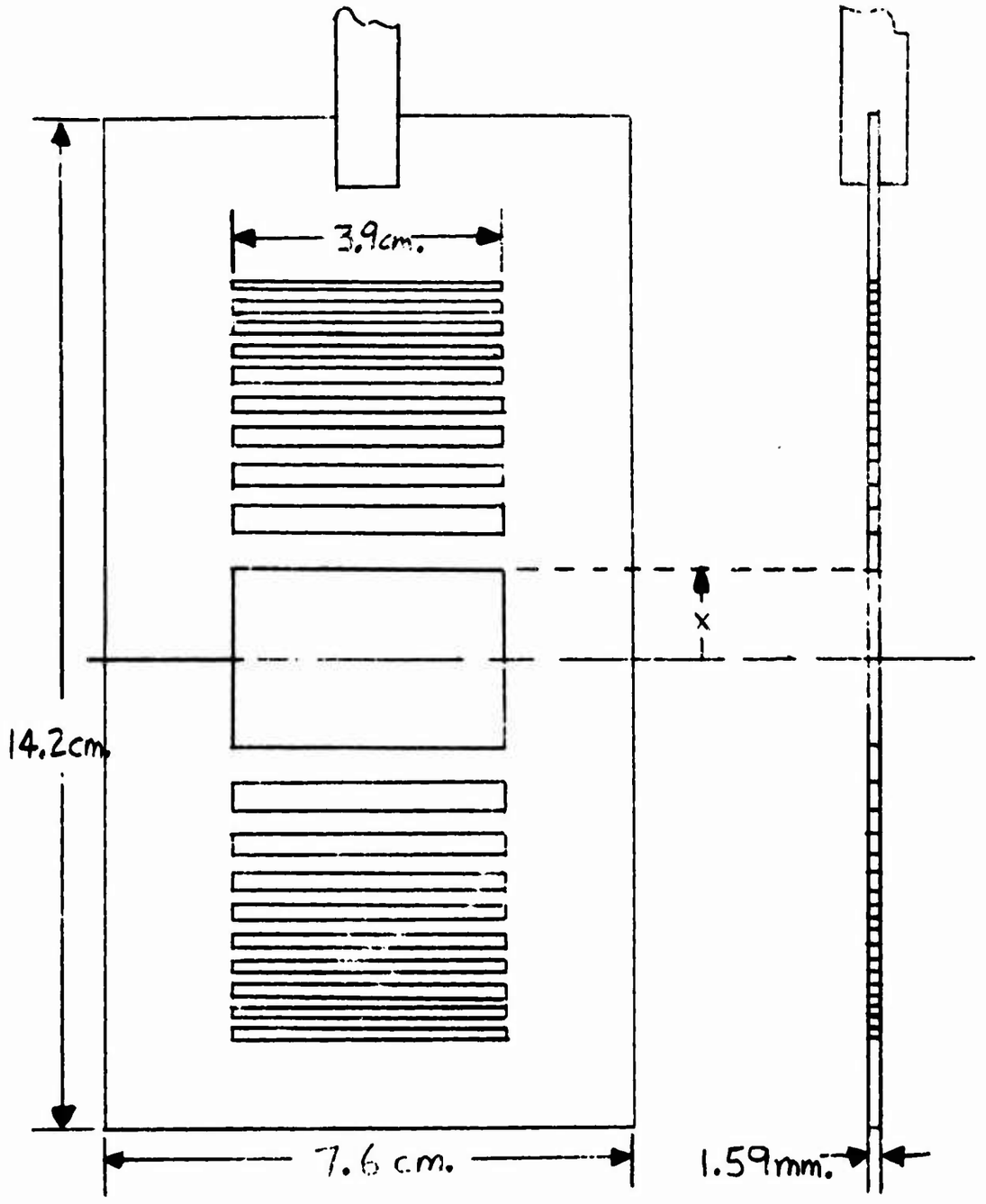

Figure 8. Design of the Ultrasonic Zone Plate.

Consider the Fresnel zone of the central slit. This is normally defined as the region in which the contributions of horizontal elements in the slit produce an interference pattern. The limit of the pattern along the axis is the point at which contributions from the opposite sides of the slit are in phase because of a path difference of one wavelength. At greater distances the difference in path length will always be less than a wavelength, and the contributions will never be in phase again. If the width of the central slit is c, it is easy to show that the distance b to the end of the Fresnel zone of a single slit is given by:

$$b = \frac{c^2 - 4\lambda^2}{8\lambda} \qquad (12)$$

Experimental Procedure

The experimental setup was similar to that given for the exponential horn in Fig. 4. The only difference is that the focus of the zone plate was in the test area in place of the horn. In fact, the first frame was taken with the zone plate in the test area. The crystal and zone plate were moved 1.5 cm. away from the test area between succeeding frames. This gave photographs of the sound field past the zone plate which overlapped each other.

Discussion of Results

The photograph obtained by piecing together those photographs from the eleven frames taken is shown in Fig. 4. The zone plate is the vertical black strip to the left. Markers show up approximately 1.6 cm. apart along the bottom of the photograph. The narrow black lines to

the left of the zone plate are standing waves caused by the reflection from the surface of the zone plate.

The zone plate was designed with equation (11) using a = 10 cm. and λ = 0.149 cm. for 1 m.c. This means, of course, that if the assumption of plane waves is good, the focus should be found 10 cm. from the zone plate. The focus shown in Fig. 9 is located at approximately 8.6 cm. Evidently, the assumption of plane waves is not exact. This is to be expected since the crystal is not a point source and was not located far enough away to approximate an infinite distance. The exact position of the focus is not easy to determine. The focus was taken to be directly above the ninth marker.

Using equation (12) to calculate the end of the Fresnel zone of the central slit, it is found that it should be 4.92 cm. from the zone plate. In Figure 9 the regularity of the pattern seems to give out just above the fourth marker (2.85 cm.). However, reflections make it impossible to tell whether the zone extends beyond this. The determination of the Fresnel zone would be made easier if the central slit were all within the photograph. The slit is 2.44 cm. wide, while the photograph covers only 1.73 cm. in a vertical direction. Not only will reflections in the tank destroy the regular pattern in the Fresnel zone of the central slit, but also interference with waves from nearby slits may contribute to its destruction, particularly at greater distances near the end of the zone. The photograph does make it clear, however, by the regular pattern near the plate, that such a zone does exist.

Figure 9. Schlieren Photograph of the Focus of the Ultrasonic Zone Plate.

III. SUMMARY AND CONCLUSIONS

Photographs of the ultrasonic wave field inside an exponential horn indicates that the simplest configuration of a plane wave source radiating into the large end of the horn produces an interference pattern throughout the horn. At the maxima of this pattern are to be found the large intensities expected. However, the photographs show that the largest intensity is to be found inside the horn. If the interior of the horn is accessible for study of finite amplitude effects, then this would not be a disadvantage. A more desirable procedure, however, would be to use a concave transducer which would produce spherical (or cylindrical) wave fronts at the mouth. This would eliminate the interference maxima inside the horn and produce the highest intensities at the throat. Such transducers can be made from a barium titanate ceramic which can be molded into the desired shape.

The photograph of the focus of the ultrasonic zone plate indicates that high intensities could be produced at the focus. It would be desirable to use the present zone plate with a larger transducer having the same area as the zone plate. Alternatively, a smaller zone plate could be constructed to be used with the present transducers. Either alternative would make the assumption of plane waves more nearly correct. If a focus to a point is desired rather than a focus to a line, a zone plate could be constructed with circular zones like the familiar optical zone plates.

BIBLIOGRAPHY

Bergmann, L., Der Ultraschall, (S. Hirzel Verlag, Stuttgart, 1954).

Gessert, W. L., "A Study of Different Ultrasonic Stroboscopes and Their Usefulness for the Study of Wave Propagation and Acoustic Birefringence," Ph. D. Thesis, Department of Physics and Astronomy, Michigan State College (1954).

Gladstone, J. H. and T. P. Dale, Phil. Trans., 153, 337 (1863).

Hiedemann, E. A., Ultraschallforschung, (Walter De Gruyter and Co., Berlin, 1939).

Hiedemann, E. A. and M. A. Breazeale, J. Opt. Soc. Am., 49, 372 (1959).

Jenkins, F. A. and H. E. White, Fundamentals of Optics, (3rd edition, McGraw-Hill Book Company, Inc., New York, 1957).

Kinsler, L. E., and A. R. Frey, Fundamentals of Acoustics, (2nd edition, John Wiley and Sons, Inc., New York, 1950).

Krasilnikov, V. A., Sound and Ultrasound Waves, (Israel Program for Scientific Translations, Jerusalem, 1963).

Makarov, L. O., "Method of Design of Rod-Type Exponential Ultrasonic Concentrators," Vol. 1 of Soviet Progress in Applied Ultrasonics, ed. V. F. Nozdreva (Consultant's Bureau, New York, 1964).

Mason, W. P. and R. F. Wick, J. Acoust. Soc. Am., 23, 209 (1951).

Morse, P. M., Vibration and Sound, (2nd edition, McGraw-Hill Book Company, Inc., New York, 1948).

Naugolnykh, K. A., J. Acoust. Soc. Am., 36, 1442 (1964).

Zankel, K. L., and E. A. Hiedemann, J. Acoust. Soc. Am., 31, 44 (1959).

Wave Interactions at Plane Boundaries

A. L. Van Buren
Department of Physics
The University of Tennessee

Correction to p.p. 83-86 of Thurston's "Wave Propagation in Fluids and Normal Solids" in Physical Acoustics, Vol. I, Part A, Edited by Mason.

This memo is intended to give a correct set of equations describing wave interaction at plane boundaries. The general case is considered of a wave incident on the boundary between two media, each of which can support both shear and longitudinal waves. The first case considered is a shear wave incident on the boundary. The treatment of Thurston is correct through equation 369, page 33; at this point he makes a wrong definition of the normal stress. The correct normal stress to consider is T_{yy}. We begin immediately after Eq. 369:

From Eq. (327) with $T_{ij} = o_{ij}$ and $S = S_o$, the shear and normal stresses on the interface are

$$T_{yx} = \mu \left(\frac{\partial u}{\partial Y} + \frac{\partial v}{\partial X} \right)$$

$$T_{yy} = \lambda' \left(\frac{\partial u}{\partial X} + \frac{\partial v}{\partial Y} \right) + 2u \frac{\partial v}{\partial y} \quad . \tag{370}$$

Continuity of u, v, T_{yx}, and T_{yy} at the interface leads to a set of four

linear algebraic equations from which the amplitude ratios can be determined. Denoting the complex amplitude Ratios by

$$t \equiv \frac{S_t}{S_I}, \quad r \equiv \frac{S_r}{S_I}, \quad T \equiv \frac{L_t}{S_I}, \quad R \equiv \frac{L_r}{S_I} \tag{371}$$

and introducing also the abbreviations

$$Z = \frac{\rho_2 V_2}{\rho_1 V_1}, \quad f_2 = \frac{V_p^2}{V_2}[\cos 2\theta_t], \quad f_1 = \frac{V_{p1}}{V_1}[\cos 2\theta]$$

we may put the set of equations for the amplitude ratios in the following matrix form:

$$\begin{vmatrix} Z\sin 2\theta_t & -\sin 2\theta & -Zf_2 & -f_1 \\ Z\cos 2\theta_t & \cos 2\theta & 2Z\sin\theta_t\cos\theta_{1t} & -2\sin\theta\cos\theta_{1r} \\ -\cos\theta_t & \cos\theta & -\sin\theta_{1t} & -\sin\theta_{1r} \\ \sin\theta_t & \sin\theta & -\cos\theta_{1t} & \cos\theta_{1r} \end{vmatrix} \begin{vmatrix} t \\ r \\ T \\ R \end{vmatrix} = \begin{vmatrix} \sin 2\theta \\ \cos 2\theta \\ -\cos\theta \\ \sin\theta \end{vmatrix} \tag{373}$$

For a given incident wave, the directions of the reflected and refracted waves can be obtained from Eq. (366), and their amplitudes can be obtained from Eq. (373). The additional discussion will be limited to the most important special case - that of a traction-free boundary, i. e., the case when there is no second medium.

In this case it is easily shown that r and R can be obtained

from Eq. (373) by setting Z = 0. We then have the pair of equations

$$\begin{aligned} -r \sin 2\theta - f_1 R &= \sin 2\theta \\ r \cos 2\theta - 2R \sin\theta \cos\theta_{1r} &= \cos 2\theta \end{aligned} \tag{374}$$

There are two angles of incidence for which R = 0: normal incidence ($\theta = 0$, $r = 1$), and incidence at 45° ($\theta = 45^\circ$, $r = -1$).

For incidence at exactly the critical angles $\left[\sin\theta = (V_1/V_{p1})\right]$, we have $f_1 = \left[\cos 2\theta/\sin\theta\right]$, $\cos\theta_{1r} = 0$, and Eq. (374) implies $r = 1$ and $R = \dfrac{-2\sin\theta \sin 2\theta}{\cos 2\theta}$. This indicates a longitudinal wave traveling parallel to the free surface, its amplitude being somewhat less than twice that of the incident shear wave.

Beyond the critical angle, the solution applies formally with $\sin\theta_{1r}$ still given by Eq. (366), but since $\sin\theta_{1r} > 1$, θ_{1r} itself is complex with, in accordance with Eq. (313), a purely imaginary cosine given by

$$\cos\theta_{1r} = -j\left|\sqrt{\sin^2\theta_{1r} - 1}\right|$$

thus,

$$jYB_{1y} = jY\left(-j\frac{\omega}{V_{p1}}\left|\cos\theta_{1r}\right|\right) = \frac{Y\omega}{V_{p1}}\left|\cos\theta_{1r}\right| .$$

This means that the dilatational part of the disturbance in Eq. (368) dies away exponentially with increasing distance below the surface.

3. LONGITUDINAL WAVES

Just as in the preceding case, an incident longitudinal wave gives rise to reflected and refracted waves of both types. We represent the incident wave by

$$\vec{U}_I = \vec{N}_I L_I \exp\left[j\omega\left(t - \frac{\vec{N}_I \cdot \vec{r}}{V_{p1}}\right)\right]$$

where N is again given by Eq. (300). Transmitted and reflected shear and longitudinal waves can be represented by Eqs. (362) and (363). Then Eq. (365) holds except that the first equation is replaced by

$$\vec{U}_1 = (\vec{i}\sin\theta + \vec{j}\cos\theta)L_I \exp\left[j\omega\left(t - \frac{Y\cos\theta + X\sin\theta}{V_{p1}}\right)\right]$$

In place of Eq. (366), we find

$$\frac{\sin\theta}{V_{p1}} = \frac{\sin\theta_t}{V_2} = \frac{\sin\theta_r}{V_1} = \frac{\sin\theta_{1t}}{V_{p2}} = \frac{\sin\theta_{1r}}{V_{p1}} \qquad (375)$$

Hence, $\theta_{1r} = \theta_1$ sines greater than unity can be handled as before. However, this is possible only of the transmitted waves, since $V_1 < V_{p1}$.

Figure 15 illustrates the angles in Eq. (375). In this case it is convenient to define

$$V_x \equiv \frac{V_{p1}}{\sin \theta}. \tag{376}$$

then the (X,t) dependence is always given by the factor

$$e^{j\omega (t-X/V_x)}.$$

The displacement components in medium 2 are still given by Eq. (369).

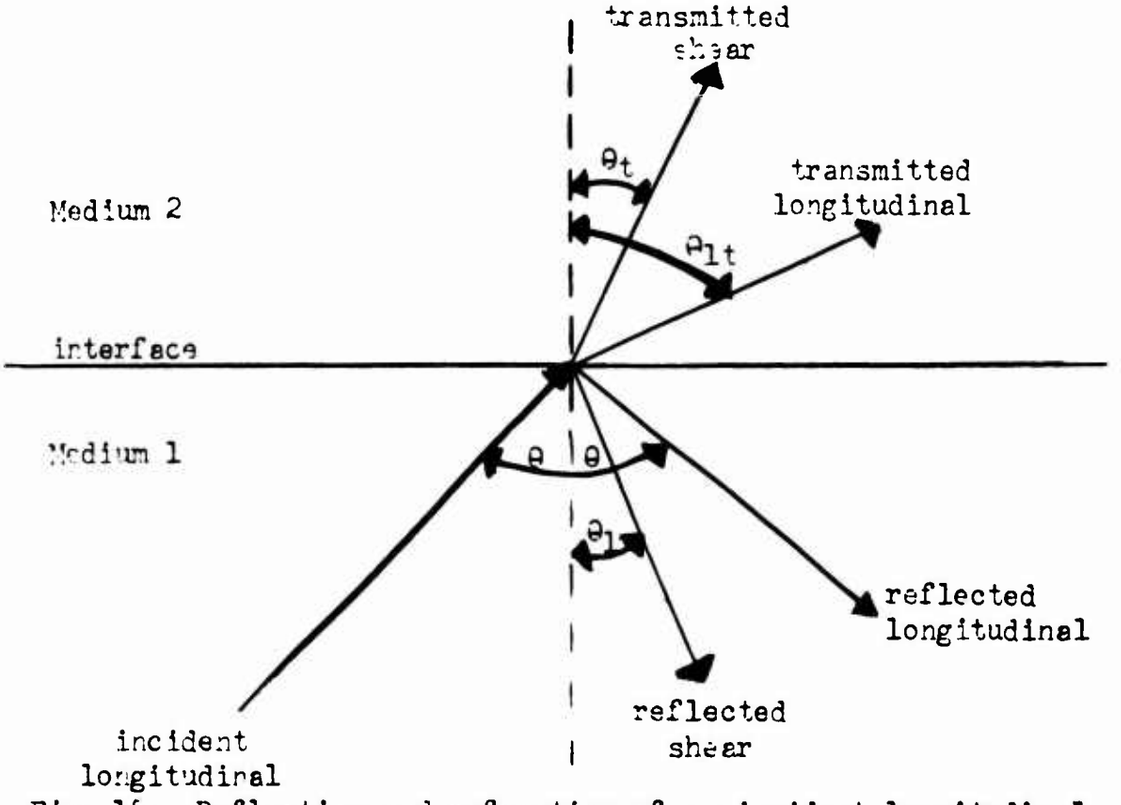

Fig. 15. Reflection and refraction of an incident longitudinal wave at the interface between two solids.

To express the displacement components in medium 1, we redefine

$$\beta_{1y} \equiv \frac{\omega \cos \theta_r}{V_1} \tag{377}$$

and use the other abbreviations in Eq. (367), recalling $\theta = \theta_{1r}$:

$$u = \exp[j\omega(t-\frac{X}{V_x})]\ [\sin\theta\ (L_I e^{-jYB_{1y}} - L_r e^{jYB_{1y}}) + S_r e^{jY\beta_{1y}} \cos\theta]$$

$$v = \exp[j\omega(t-\frac{X}{V_x})]\ [\cos\theta\ (L_I e^{-jYB_{1y}} + L_r e^{jYB_{1y}}) + S_r e^{jY\beta_{1y}} \sin\theta]. \tag{378}$$

continuity of u, v, T_{yx}, and T_{yy} at the interface again leads to a set of four linear algebraic equations for the amplitude ratios with the abbreviations

$$t \equiv \frac{S_t}{L_I},\quad r = \frac{S_r}{L_I},\quad T = \frac{L_t}{L_I},\quad R = \frac{L_r}{L_I},\quad Z = \frac{\rho_2 V_2}{\rho_1 V_1},\quad f_2 = \frac{V_{p2}}{V_2}\left[\cos 2\theta_t\right], \tag{379}$$

$$f_1 = \frac{V_{p1}}{V_1}\left[\cos 2\theta_r\right].$$

The equations take the following form:

$$\begin{vmatrix} \cos\theta_t & -\cos\theta_r & \sin\theta_{1t} & \sin\theta \\ \sin\theta_t & \sin\theta_r & -\cos\theta_{1t} & \cos\theta \\ -Z\sin 2\theta_t & \sin 2\theta_r & Z f_2 & 1 \\ Z\cos 2\theta_t & \cos 2\theta_r & \frac{V_2}{V_{p2}} Z\sin 2\theta_{1t} & -\frac{V_1}{V_{p1}}\sin 2\theta \end{vmatrix} \begin{vmatrix} t \\ r \\ T \\ R \end{vmatrix} = \begin{vmatrix} \sin\theta \\ -\cos\theta \\ f_1 \\ \frac{V_1}{V_{p1}}\sin 2\theta \end{vmatrix} \tag{380}$$

The special case of a free surface ($Z = 0$) has been discussed in detail by Arenberg (16). Some of the most important results were summarized by Mason (9, pages 23-26).